npj | Systems Biology and Applications

www.nature.com/npjsba

ARTICLE OPEN

Osmolyte homeostasis controls single-cell growth rate and maximum cell size of *Saccharomyces cerevisiae*

Tom Altenburg[1,2,3], Björn Goldenbogen[1,3], Jannis Uhlendorf[1] and Edda Klipp[1*]

Cell growth is well described at the population level, but precisely how nutrient and water uptake and cell wall expansion drive the growth of single cells is poorly understood. Supported by measurements of single-cell growth trajectories and cell wall elasticity, we present a single-cell growth model for yeast. The model links the thermodynamic quantities, such as turgor pressure, osmolarity, cell wall elasto-plasticity, and cell size, applying concepts from rheology and thin shell theory. It reproduces cell size dynamics during single-cell growth, budding, and hyper-osmotic or hypo-osmotic stress. We find that single-cell growth rate and final size are primarily governed by osmolyte uptake and consumption, while bud expansion requires additionally different cell wall extensibilities between mother and bud. Based on first principles the model provides a more accurate description of size dynamics than previous attempts and its analytical simplification allows for easy combination with models for other cell processes.

npj Systems Biology and Applications (2019)5:34 ; https://doi.org/10.1038/s41540-019-0111-6

INTRODUCTION

Cells are exposed to hydrostatic pressure driven by the difference between inner and outer osmolarity. For example, at the boundaries of tissues in higher eukaryotes, cells often encounter a wide range of osmotic changes due to cytokines, hormones, etc. Similarly, unicellular organisms such as the eukaryotic model organism *Saccharomyces cerevisiae* or yeast, proliferate under a wide range of osmotic conditions caused, for example, by periods of rain or drought. In the presence of these changing conditions yeast has evolved strategies to maintain cellular integrity, ranging from regulating intracellular osmolarity to constructing elastic scaffolds such as the cytoskeleton or the cell wall. Water flow over the cell membrane follows the osmotic and hydrostatic pressure differences[1] and, therefore, impacts cell size, according to the cellular deformability. Therefore, yeast on the one hand, has to adapt its internal osmotic pressure to external conditions[2–4] to prevent bursting as well as critical shrinking, on the other hand has to regulate its growth rate. The uptake and subsequent metabolization of nutrients provides not only building blocks and energy for the synthesis of new cell material, but also change the internal osmolarity and thereby can drive inward water flux, which in turn can lead to an increase in cell size. In walled cells, such as Baker's yeast or plant cells, the difference between internal and external osmotic pressures are counteracted by turgor pressure arising from elastic expansion of cell wall material. Turgor pressure prevents exaggerated swelling and maintains cell shape. Although reported values of turgor pressure in yeast range from 0.1 to 1.0 MPa,[5,6] more recent single-cell measurements suggested a value of 0.2 MPa.[7]

Several studies have already addressed aspects of osmoregulation and single cell growth concomitantly, however, the mutual influence of both processes remained poorly understood. In a previous model, thermodynamic descriptions of volume and pressure changes were integrated within the osmotic stress response system, i.e. the high osmolarity glycerol (HOG) signaling pathway, metabolism, and gene expression.[3] This integrative model permitted predictions regarding the effect of several gene-knockouts on volume dynamics. Another model integrated further published data with biophysical and mechanical properties of yeast to describe the loss in volume immediately after osmotic stress.[4] Both models explain volume regulation following a hyperosmotic shock, but are not designed to describe the small and steady volume variations during normal growth.

Although various volume regulation models have been proposed, a unified understanding of the interplay between cell mechanics, turgor, volume, and metabolism during growth and perturbations, e.g. osmotic shocks, is still missing. Earlier approaches focused solely on animal cells, where cellular integrity is maintained by the cytoskeleton.[8,9] However, mammalian cells can also face high osmotic pressure changes and cell integrity of certain species is supported by external structures, such as matrix, mucus or wax, which fulfill similar functions as a cell wall.

Here, we present a single-cell growth model (SCGM), which focuses on the interplay of three thermodynamic quantities: cell volume, osmolarity, and turgor pressure, and which covers growth and budding of single yeast cells as well as the response to external osmotic variations. We further tested the model against single-cell growth data from brightfield microscopy images and used atomic force microscopy (AFM) to gain information on the cell wall elasticity during budding. The model combines different concepts, such as cell wall mechanics in yeast[10–15] rheology, a subfield of continuum mechanics and broadly used in plant physiology[16–19] and applied to fungi,[20,21] thin shell theory,[22–24] water homeostasis and dynamics,[1,25] and osmoregulation (in general or exemplified by HOG).[3,26,27] The SCGM is capable of describing both drastic volume variations caused by hyperosmotic or hypoosmotic shocks, as well as relatively small but steady gains in cell size during growth. To demonstrate that the SCGM can be combined with models for cellular signaling and metabolism, we introduced the HOG signaling cascade model[27] as an exemplary pathway that plays a major role in yeast osmoregulation.[2]

[1]Theoretical Biophysics, Humboldt-Universität zu Berlin, Berlin, Germany. [2]Robert Koch-Institut, Berlin, Germany. [3]These authors contributed equally: Tom Altenburg, Björn Goldenbogen. *email: edda.klipp@rz.hu-berlin.de

RESULTS

The SCGM combines formalisms for turgor pressure, osmoregulation, and cell wall mechanics

Cellular volume varies according to material accumulation and water flux across the cell membrane, which follows the osmotic and hydrostatic pressure gradient. For volume flux and the conversion from osmolarity to osmotic pressure, we considered established formalisms described by Kedem–Katchalsky and Boyle van't Hoff.[1,3,25,27] To this end, we defined total cell size $V_t = V_{os} + V_b$ as the sum of the osmotic volume V_{os}, which is sensitive to osmotic or hydrostatic pressures changes, and the solid volume V_b, which is not affected by water dynamics, e.g. volume occupied by macromolecules (see Fig. 1a). In a confined system, such as a cell, the outward-directed water flux over the boundary, the cytoplasmic membrane, must equal the negative change in volume of this system over time:

$$\dot{V}_{os} = -J_w$$

According to Kedem–Katchalsky, water flux J_w across the membrane is proportional to the causative force, i.e. pressure differences, and is thus defined as

$$J_w = L_p G(\Pi_t + \Pi_e - \Pi_i),$$

where L_p denotes the hydraulic conductivity of the membrane per unit area, G is the area of the cell surface, Π_t is the turgor pressure and Π_e and Π_i are the external and internal osmotic pressures. Turgor pressure is typically calculated under a steady-state assumption of negligible water fluxes ($J_w = 0$) and, hence, equals the difference between external and internal osmotic pressures. To capture the dynamics of volume variation, we went a step further by neither constraining J_w nor the total number of particles in the system, thereby establishing distinct mathematical descriptions for the three main quantities: volume, turgor pressure, and osmolarity. The osmotic pressures Π_e and Π_i depend on the the internal and external osmolyte concentrations c_i and c_e according to Boyle van't Hoff's equation:

$$\Pi_i = c_i RT \text{ and } \Pi_e = c_e RT,$$

where R is the gas constant and T the temperature. While c_e was assumed to be unaltered by the processes of a single cell, c_i changes with the uptake and dilution of osmolytes, such as nutrients and ions. Particularly, osmolyte uptake was assumed to be proportional to the cell surface G, over which osmolytes must be transported, while consumption of osmolytes was assumed to be proportional to the cell volume V. Further, volume expansion must lead to a dilution of osmolytes, hence to a decrease in c_i. Combined, we obtain the following simplified description of osmolyte dynamics within the cell:

$$\dot{c}_i = \frac{1}{V}(k_{uptake} G - k_{consumption} V - c_i \dot{V}),$$

with the proportionality constants k_{uptake} and $k_{consumption}$. This basic description can be extended, if a more detailed metabolism model is at hand, as we exemplify below for osmotic stress response by including the HOG pathway and glycerol accumulation.

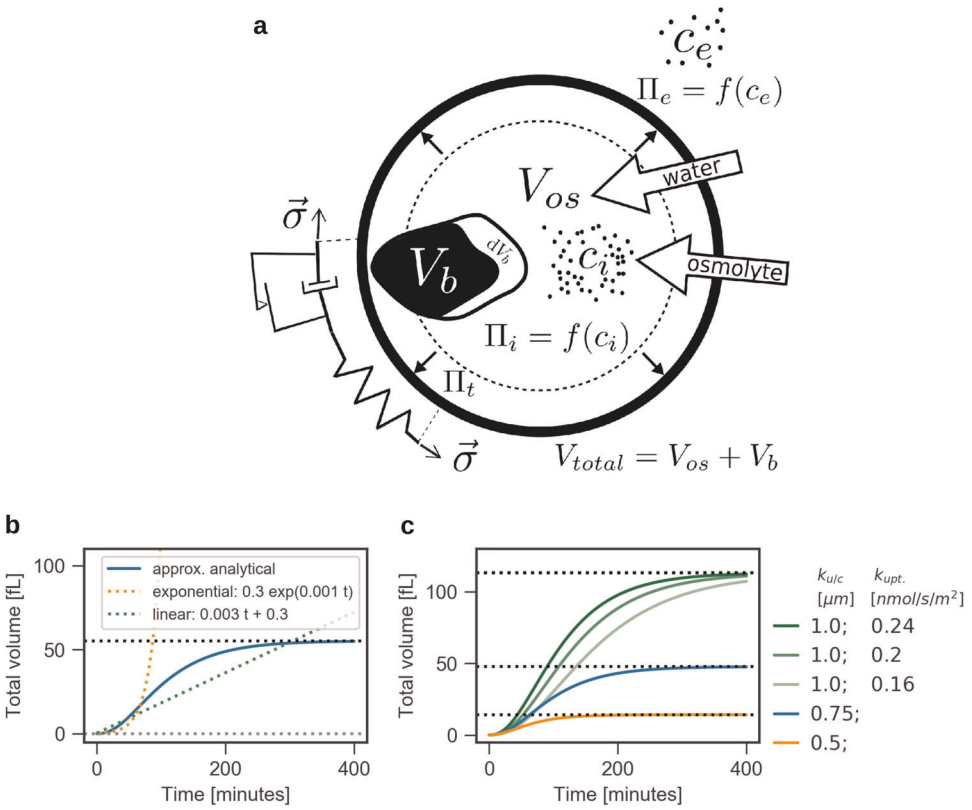

Fig. 1 The single-cell growth model (SCGM) predicts non-linear growth behavior. **a** Sketch of the SCGM. The cell volume is separated into an osmotic active volume V_{os}, accessible for solubles, V_{os} and a soluble-inaccessible volume V_b. Uptake of osmolytes over the membrane increases the internal osmolyte concentration c_i and thereby the internal osmotic pressure Π, which drives water influx and thus expands the cell. Volume expansion, in turn, is limited by the elasto-viscoplastic cell wall (represented as mechanical circuit). **b**, **c** Volume trajectory for an individual yeast cell. **b** The SCGM (blue line) shows different volume trajectories compared to linear (green dotted line) or exponential (orange dotted line) growth. **c** Varying uptake and consumption equally ($k_{u/c}$ = const.), leaves final cell size $V_{final}(t \to \infty)$ unaffected, but changes growth rate (green lines). Alterations of ratio $k_{u/c}$ affects final cell size V_{final} with $V_{final} = 12\pi(k_{u/c})^3$

Having derived descriptions for the dynamics of the volume and inner osmolarity, we required further a description for the turgor pressure. Given that the turgor pressure equals hydrostatic pressure acting on the cell wall, the main structural element of the yeast cell, the cell wall and its mechanical properties must be considered in our description. For simplification, we assumed the cell wall to be a thin spherical shell with radius r. The cell wall expands elastically or plastically depending on forces it is exerted to. While an elastically expanded volume relaxes to its initial size when the pressure vanishes, plastic expansion is irreversible. Taking a constant wall thickness into account, the irreversible expansion can also been interpreted as cell growth, where new cell wall material has to be provided by the cell wall synthesis machinery. Assuming a linear constitutive relationship for elasticity, the deformation of the cell volume, i.e. strain $\varepsilon_{\text{Hook}}$, scales linearly with turgor pressure in a purely elastic cell wall.

$$\varepsilon_{\text{Hook}} = \frac{1-\nu}{E}\frac{\Pi_t r}{2d}.$$

Here, E is the Young's modulus, representing the elasticity of the cell wall, v is the Poisson's ratio, and d is the thickness of the cell wall. Consequently, water influx will lead to an increase in r and hence directly to larger strain inside the cell wall. Note that cell wall thickness is assumed to be constant and therefore depended neither on the radius r nor on the time t.

In contrast to elastic deformation, plastic deformation was assumed to occur only above the critical turgor pressure Π_{ct} and instead of the strain, the strain rate is proportional to the acting pressure with a factor ϕ. Whereby ϕ represents the extensibility of the cell wall. The strain rate reads

$$\dot{\varepsilon}_{\text{Bingham}} = \frac{\phi r}{2d} f_m(\Pi_t, \Pi_{ct}),$$

$$\text{where} \quad f_m(\Pi_t, \Pi_{ct}) = \begin{cases} \Pi_t - \Pi_{ct} & \text{if} \quad \Pi_t \geq \Pi_{ct} \\ 0 & \text{else} \end{cases}.$$

To reflect elastic and plastic behavior of the cell wall, we used a mechanical model of the cell wall, in which a Hookean and a Bingham element, representing the elastic and plastic response, are coupled in series (Fig. 1a). Then the total strain is the sum of the strains of each element $d\varepsilon = dr_{\text{Hook}}/r + dr_{\text{Bingham}}/r$. Taking the time derivative $\dot{\varepsilon}$ of the total strain enabled us to combine descriptions for both mechanical elements in a single ODE for the change in turgor pressure over time $\dot{\Pi}_t$ (for details see Supplementary Note 1):

$$\dot{\Pi}_t = \frac{2Ed}{1-\nu}\frac{\dot{r}}{r^2} - \Pi_t\frac{\dot{r}}{r} - \frac{E\phi}{(1-\nu)} f_m(\Pi_t, \Pi_{ct}).$$

Models that include two of the three terms of this equation have already been applied in other turgor-related models.[16,18,19,28] A comparison with the previously proposed description of turgor in plant physiology[19] revealed, that the additional term resulted from the geometric description of the cell as a thin spherical shell, in particular when calculating the time derivative of the elastic element.

Cell expansion is therefore mainly influenced by two processes: first, the control of internal osmolarity c_i by uptake, dilution, and consumption of osmolytes, which together with turgor pressure Π_t drive water influx and outflux J_w, and hence determine the water volume in the cell (V_{os}), and second, the elasto-plastic deformation of the cell wall due to turgor pressure. The water influx $J_w < 0$ expands the cell wall elastically and thereby increases turgor pressure. When turgor pressure exceeds the critical value Π_{ct}, the cell wall starts to yield, e.g. the cell wall expands irreversibly and the cell grows. Yielding leads to relaxation of stress in the cell wall and in turn to a decrease in turgor pressure, facilitating further influx of water. Hence, growth typically proceeds close to, but not at steady state ($J_w = 0$), where water and osmolyte influxes are balanced by turgor dynamics.

Summarizing, the basic SCGM comprises three coupled ODE's for volume, turgor pressure, and internal osmolarity. Key parameters and initial values for simulation or analytic solution are listed in Table 1. The temperature was set to $T = 303$ K, i.e. the optimal growth temperature for yeast and our experimental standard condition. The external osmolyte concentration c_e was set to 240 mM, the mean value for our standard growth medium.

Considering a cell growing without any osmotic perturbations, the SCGM can be reduced to a simpler description of cell size development. Simulations revealed that without osmotic stress, internal osmolarity c_i and turgor pressure Π_t approach steady states. In this case the SCGM can be solved analytically (Fig. 1b, Supplementary Fig. 1). We obtained an implicit differential equation F comprising the time derivative of the radius $\dot{r}(t)$, the time-dependent function of cellular radius $r(t)$, steady states and time:

$$F(\dot{r}, c_i^{SS}(r(t)), \Pi_t^{SS} = \Pi_{ct}, t) = 0,$$

where c_i^{SS} is a quasi-steady state for internal osmolarity (quasi-,

Table 1. Parameters and initial values

Parameter	Value	Unit	Description	Source
r_b^0	0.3	µm	Init. radius (non-osmolytic volume)	Assumption
r_b^0	0.1	µm	Init. radius (osmolytic volume)	Assumption
c_i^0	319.17	mM	Osmolyte concentration (internal)	Calculated from turgor pressure
c_e	240.0	mM	Osmolyte concentration (external)	Measured
Π_t^0	2.0×10^5	Pa	Initial turgor pressure	[7]
R	8.314	$\frac{J}{mol\,K}$	Ideal gas constant	
T	303.0	K	Temperature	
L_p	1.19×10^{-6}	$\frac{\mu m}{sPa}$	Membrane water permeability	[3]
Π_{tc}	2.0×10^5	Pa	Critical turgor pressure	[7]
d	0.115	µm	Cell wall thickness	[63]
ϕ	1.0×10^{-3}	$\frac{1}{sPa}$	Extensibility	Initial assumption, fit in Fig. 4
v	0.5	–	Poisson's ratio	
E	2.58×10^6	Pa	Young's modulus (3D)	[7]
k_{uptake}	2.0×10^{-16}	$\frac{mmol}{\mu m^2 s}$	Osmolyte uptake rate constant	Initial assumption, fit in Fig. 4
$k_{consumption}$	2.0×10^{-16}	$\frac{mmol}{\mu m^3 s}$	Osmolyte consumption rate const.	initial assumption, fit in Fig. 4

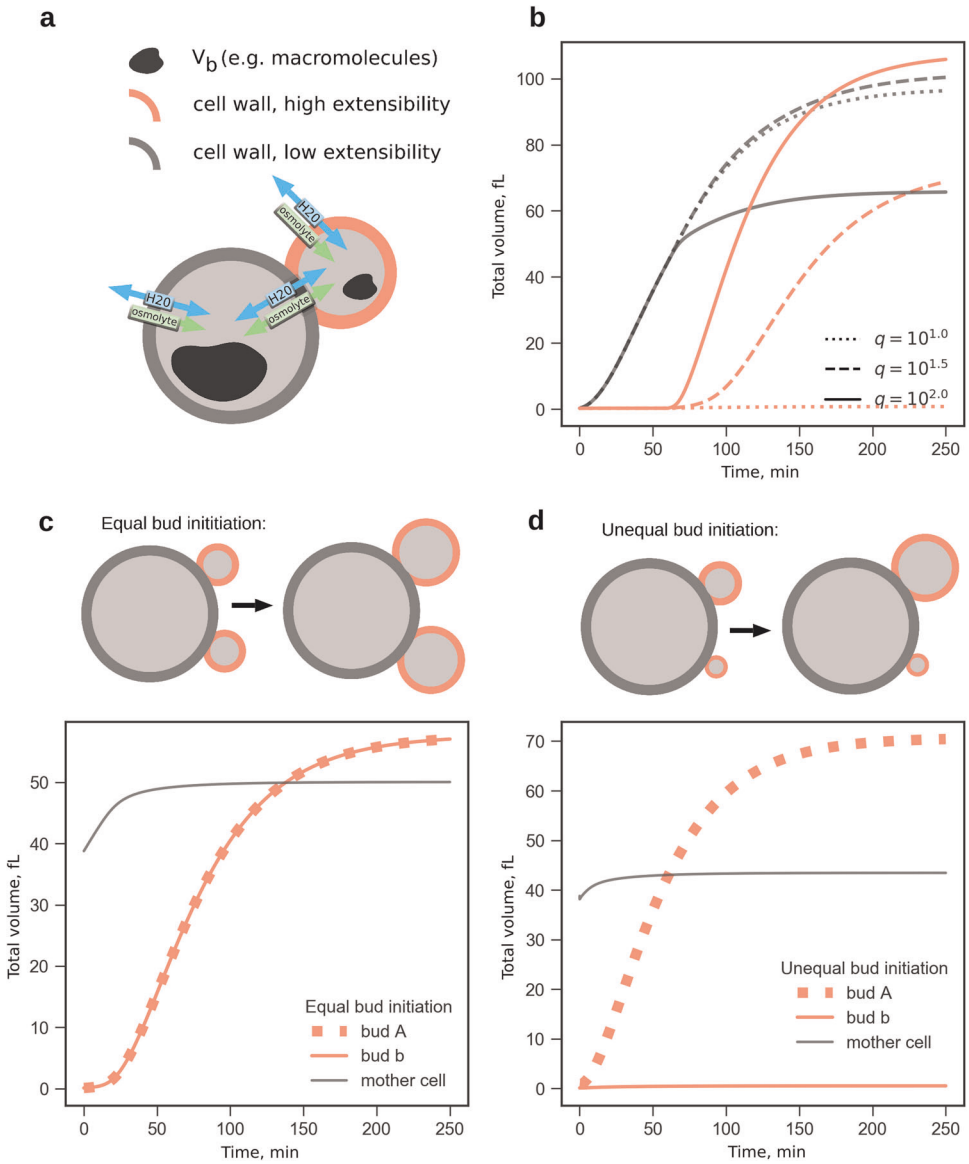

Fig. 2 Bud expansion driven by cell wall anisotropy and a possible protection mechanism against two-bud growing malfunction. **a** Two volume model instances were interconnected via water and osmolytes fluxes. The coupled model accounts for different cell wall extensibilities ϕ between bud and mother. **b** Volume dynamics are shown for mother and bud for three different extensibility ratios $q = \phi_{\mathrm{bud}}/\phi_{\mathrm{mother}}$. Bud expansion is possible only at $q > 10$. **c** To investigate two-bud growing mutants, two bud instances linked to a mother cell were initialized with equal bud sizes. Both buds have identical volume dynamics. **d** Effect of unequal initial bud sizes: differences are amplified and only the larger bud grows

because still depends on $r(t)$) and Π_t^{SS} the steady state for turgor pressure, which equals critical turgor pressure Π_{ct} during growth. Solving F (Supplementary Note 3), we first, identified a limes of cellular radius for long times scales:

$$r_{\mathrm{final}} = \lim_{t\to\infty} r(t) = 3\frac{k_{\mathrm{uptake}}}{k_{\mathrm{consumption}}}.$$

and second, obtained an analytical solution for $r(t)$. Since the resulting expression for $r(t)$ is rather complex, we approximated $r(t) \approx \tilde{r}(t)$ (for derivation see Supplementary Note 4), yielding a function for the radius of a growing cell:

$$\tilde{r}(t) = r_{\mathrm{final}} - (r_{\mathrm{final}} - r_0)e^{\frac{-k_{\mathrm{uptake}}RT}{r_{\mathrm{final}}(\Pi_{ct}+\Pi_e)}(t-t_0)},$$

where r_{final} is the final cellular radius for long time scales t, r_0 is the initial radius at time t_0. The solution points out that external osmotic pressure, critical turgor pressure and internal osmotic pressure, as well as k_{uptake} and $k_{\mathrm{consumption}}$, dictate the trajectory of cell growth. For our solution it was crucial to include the quasi-steady state $c_i^{SS}(r(t))$. In this way, the influences of k_{uptake} and $k_{\mathrm{consumption}}$ on the quasi-steady state of internal osmolarity could be propagated to the radius description $\tilde{r}(t)$. As shown in Fig. 2c, our model suggests that final cell size depends exclusively on the ratio $k_{u/c} = k_{\mathrm{uptake}}/k_{\mathrm{consumption}}$, but not on cell wall-related quantities. Scaling both rate constants equally while keeping ratio $k_{u/c}$ constant, scales growth rate, but keeps final cell size constant. The growth dynamics $\tilde{r}(t)$ depends additionally on critical turgor pressure and external osmolarity. For hyperosmotic shock response, we derived another analytical solution for turgor dynamics, which is related to the Merritt–Weinhaus equation,[29] i.e. the pressure-to-size relation of an ideal elastic thin shell (Supplementary Fig. 2 and Supplementary Note 2).

Coupled SCGM permits the description of combined growth of mother and bud

Above, we provide a description of growth dynamics for an individual cell, which is only valid for yeast cells in G1 phase (single cell without a bud). In other cell cycle phases, cells consist of two compartments (mother and bud), connected by a neck and with different growth rates.[30] To model these growth phases, we coupled two SCGMs, one each for mother and bud (Fig. 2a), in which both start with the same small initial volume, but with a time delay $t_{budstart}$ for the bud, leaving time for the mother to grow. $t_{budstart}$ represents the time between two successive bud formations and, hence, a characteristic length of the cell cycle. Both model instances were coupled by allowing water and osmolyte exchange according to the pressure and concentration differences. The coefficients for both fluxes were arbitrarily chosen such that water and osmolyte gradients vanish in the considered time scale. Apart from the mechanical cell wall properties and the initial geometry, both instances were similar, particularly in their osmolyte uptake and consumption rates, k_{uptake} and $k_{consumption}$. However, it is very unlikely that the mechanical cell wall properties are identical in both compartments, as changes in cell wall structure during budding were reported.[31] In particular, chitin incorporation into the lateral cell wall is delayed in buds until after septation. As a potentially discriminating cell wall property, we considered either the Young's modulus E or the extensibility ϕ. Systematic analysis of the impact of varying E on bud growth showed that only a strongly decreased E_{bud} compared to E_{mother} led to bud growth (Supplementary Fig. 3), though at the expense of the growth of the mother. In contrast, when varying ϕ, both compartments continued to grow (Fig. 2b), as long as ϕ_{bud} was at least $10^{1.5}$ times higher than ϕ_{mother}. Note that we focused here on biophysical principles, instead of on the complex biochemical processes governing cell division, such as cell polarization and subsequent bud emergence.

Measurements of local cell wall elasticity of mother and bud reveal a distinct difference between two asymmetric growth processes in yeast, budding and shmooing

As discussed above, a significantly lower elastic modulus of the bud cell wall could drive bud expansion in the model. Previously, we reported that such localized softening of cell wall material occurs during sexual conjugation in *S. cerevisiae*.[7] To test whether both processes, budding and sexual conjugation, follow similar underlying principles, we applied multi-parametric AFM on living yeast cells[32] as depicted in Fig. 3a. From the force-response curves of nano-indentation measurements (Fig. 3b), we obtained the local Young's modulus E. To compare mother and bud, we selected regions of equal size at each compartment (Fig. 3c, d). We avoided strongly tilted regions, compared to the scanning plane, and regions of previous budding events, so-called bud scars, which contain a higher amount of chitin and are reported to be stiffer.[33] Intriguingly, bud cell walls appeared to be stiffer, not softer, than their mothers' cell walls (Fig. 3). From a linear fit, we estimated a 1.3 0.1-fold increase in the Young's modulus from

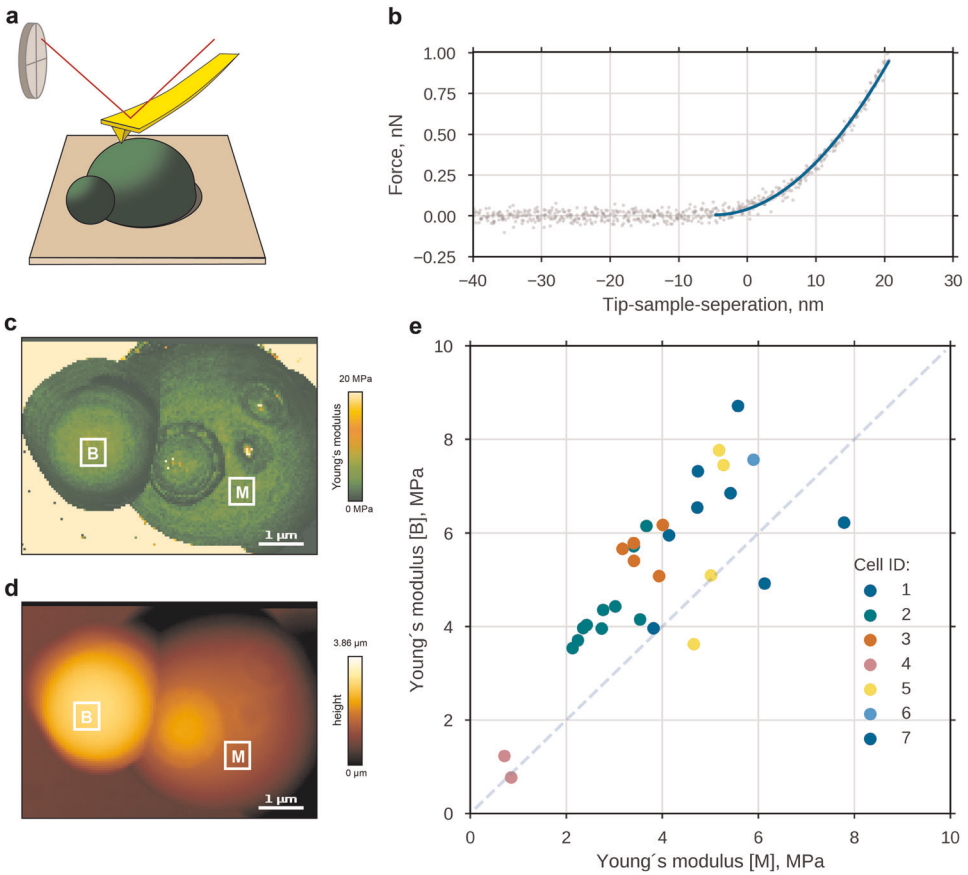

Fig. 3 Local Young's modulus of the cell wall is slightly higher for bud than for mother. **a** Experimental setup: entrapped haploid *S. cerevisiae* cells were scanned using atomic force microscopy, whereby at each image position the force response to nano-indentation was measured. **b** Exemplary approach curve for one pixel along with a Sneddon fit (blue). Obtained spatial information is shown for cell wall elasticity **c** and height **d** of a budding mother cell. For further analyses, the mean cell wall elasticities from the least curved region of mother and bud ([M] and [B]) were used, avoiding regions of former budding events, bud-scars. **e** Mean local E at buds compared to mean local E at mothers for 30 measurements on seven cells (same cells, same color). Dashed line: equal cell wall elasticities of bud and mother

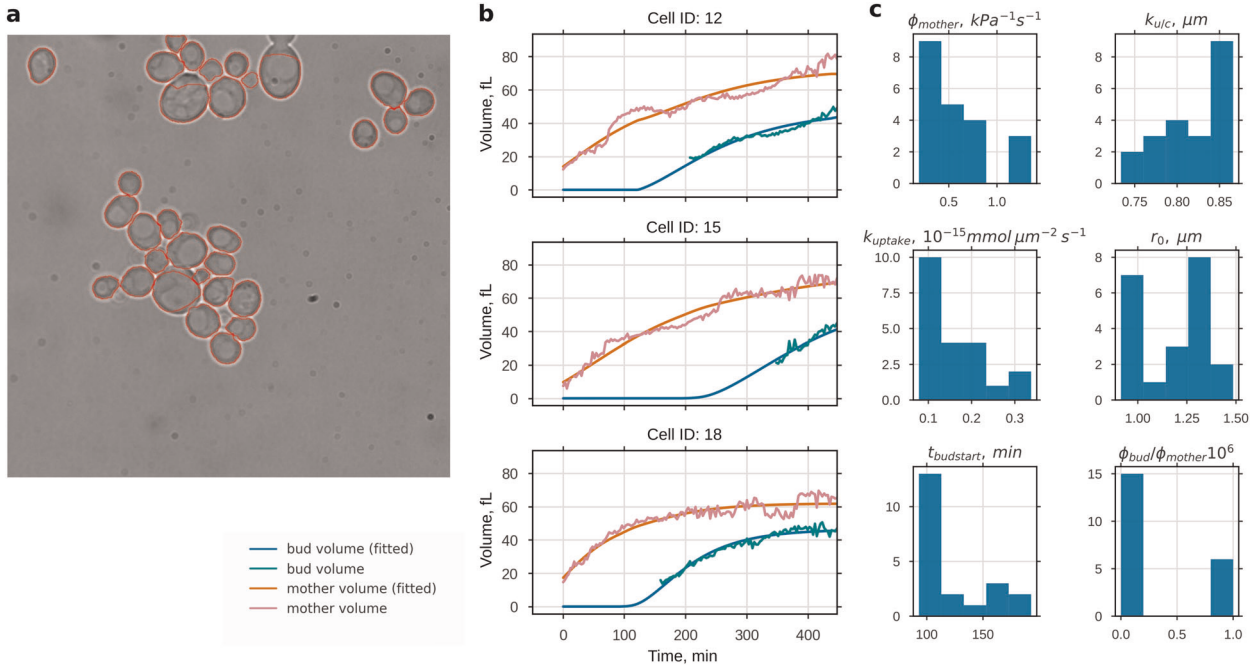

Fig. 4 Growth parameter estimation from time series of bright field microscopy images. **a** Cross-sectional areas of 21 single yeast cells were automatically detected from transmission microscopy images and followed over time. Estimated volume increases of mother and bud were used to fit the model parameters: import rate of osmolytes k_{uptake}, import and degradation ratio of osmolytes $k_{u/c}$, cell wall extensibility of the mother ϕ_{mother}, and the extensibility ratio of bud and mother ϕ_{bud}/ϕ_{mother}. Time of bud start $t_{budstart}$ and initial osmotic radius r_0 were used as free initial conditions. Three measured volume trajectories and corresponding fits are shown in **b** (for the complete data set see Supplementary Fig. 7). Histograms of the resulting parameter values are shown in **c**. Except for ϕ_{bud}/ϕ_{mother} we could assign all of the parameters with low variability, despite the high variability in the volume development in these data

mother to bud (Supplementary Fig. 6). Although the apparent stiffness at the bud cell wall could be biased by different surface curvatures, a significant cell wall softening at the bud, as measured for sexual conjugation, can be rejected. This reveals a distinct difference between two of the asymmetric growth processes in yeast, budding and sexual conjugation. Consequently, we focused on the extensibility as distinguishing feature between mother and bud cell wall.

Verification of the model against volume data from light microscopy

To test whether the coupled SCGM correctly describes the growth of single yeast cells and to estimate otherwise inaccessible parameters, we measured the growth trajectories of single yeast cells and used these to constrain model parameters. Cells were grown as monolayer in a microfluidic device, allowing observation of individual cells for long time periods (>15 h). We tracked single cells in microscopic bright field images using the software CellStar[34] and determined the first bud emergence manually for each cell (Fig. 4a). A bud neck marker (Cdc10-mKate2) was used to identify pairs of mothers and corresponding buds and to reconstruct the lineage. Knowing the lineage enabled us to collect 21 coupled volume trajectories for mother and bud. Since the time between first appearance of a cell and its first budding event varied considerably, we did not fit the model to mean growth data but to single volume trajectories instead. Figure 4b and Supplementary Fig. 7 show that the coupled SCGM is able to describe the growth pattern of single cells growing at different rates. For the growth of mother and bud, six independent parameters (mean ± s.d.) have been determined (Fig. 4c). In addition to two individual parameters (r_0 and $t_{budstart}$), we considered two global parameters (k_{uptake} and $k_{u/c}$) and two compartment-dependent parameters (ϕ_{mother} and $q = \phi_{bud}/\phi_{mother}$). r_0 was the fitted radius belonging to the initial osmotic volume of the later mother. With $\bar{t}_{budstart} = 117 \pm 33$ min the estimated mean cell cycle length differed remarkably from the time when a new bud was clearly recognizable for the first time (first green data point in Fig. 4b). When analyzing estimated rates constants for osmolyte uptake and consumption, we found that the growth rate determining k_{uptake} showed some variation between single cells ($1.59 \times 10^{-16} \pm 0.72 \times 10^{-16}$ mmol µm^{-2} s^{-1}). In contrast $k_{u/c}$, which limits the maximum volume, showed very little variation (0.82 ± 0.07 µm). Focusing on cell wall extensibility, we estimated a value of 0.57 ± 0.34 kPa^{-1} s^{-1} for the mother ϕ_{mother} and found that ϕ_{bud} needs to be at least 100 times higher. We could not determine a precise value for the extensibility ratio ϕ_{bud}/ϕ_{mother}. However, profile likelihood and sensitivity analysis (Supplementary Fig. 8) revealed that variation of ϕ_{bud}/ϕ_{mother} has no significant impact on other parameters.

For the Δ *cdc42* mutant a probability for the emergence of two buds was reported. Our model suggests that this probability (occurrence of multiple buds) is not only influenced biochemically (e.g. by Cdc42p) but also by the the passive dynamics in cell size described above. Therefore, the constellation of two small volumes connected to a main volume establishes an additional layer of filtering out stunted buds.

Analysis of volume trajectories from Garmendia-Torres et al. [35]

So far the analysis of growth parameters was based on 21 volume–trajectory pairs (*dataset 1*), which provided valuable information on the dimension of each parameter. However, for the extensibility ratio ϕ_{bud}/ϕ_{mother} only a lower boundary could be determined and the relative small sample size did not allow for decisive statements on the parameter distribution. To increase the sample size and further challenge the cSCGM we searched for single-cell data with time-resolved volume information for mother and bud and found a recent study by Garmendia-Torres et al.[35]

They reported a new microscopy-based method to investigate yeast cell-cycle and cell-size progression in parallel, by monitoring volume and histone levels of individual yeast cells. Using an automatized experimental setup they followed up to 15,000 cell cycles for each of the investigated 22 cell-cycle-related mutants. This innovative approach of tracking the fluorescence of fast maturating HTB2-sfGFP fusion proteins over time and assigning its intensity to distinct cell cycle phases, allowed them to relate the volumes of mother and bud at certain cell cycle stages to the time spent in each phase. Although this analytic approach revealed intriguing relations between cell cycle and cell size, it simplifies the dynamics of the cell size progression in the data. In particular, they assumed linear growth during the budded and unbudded phase. To shed light on this cell-size dynamics and to further challenge the cSCGM, the model was fitted to the experimental data provided by Gilles Charvin (*dataset 2*). This allowed the comparison between completely independent data sets, from different laboratories, and the analysis of data with a drastically increased sample size.

Data and data selection

The advantage of *dataset 2*, besides its dimension, is the resemblance of the used experimental and analytic approach used for *dataset 1*. In particular, yeast strain background and culture medium, BY4741 and synthetic medium supplemented by amino acids and glucose, were similar. Furthermore, the proliferation of single cells, confined to a plane using a microfluidic device, was followed at the same sampling frequency (every 3 min) using bright-field and fluorescence microscopy and volumes were calculated from cell contours, assuming ellipsoidal geometry. In contrast to *dataset 1*, *dataset 2* relied on a super-folding GFP fused to one of the histone 2B loci (HTB2-sfGFP), instead of a bud-neck marker, to monitor the cell cycle stage and to discriminate between buds and new born daughter cells. Additionally, a self-developed MATLAB software *Autotrack* for automatized cell segmentation and linage tracking, enabled to track and analyze thousands of cells in *dataset 2*.

The cSCGM was fitted to the provided volume trajectories pairs of WT yeast cells, in the same manner as described above. For better comparison with *dataset 1*, *dataset 2* was limited to the first cell cycle of new born daughter cells ($N = 6079$), i.e. cells with a replicative age of 0. Cells, defined as outliers in the data set, due to incorrect segmentation, tracking, or bud assignment to mother cells and due to insufficient fitting of histone level curves, were also neglected for further analysis. In contrast to *dataset 1*, $t_{budstart}$ was no fitting parameter but provided by the *dataset 2*. For 97% of the 6079 cells, parameter sets were found for which χ^2 was sufficiently small (Supplementary Fig. 10). Exemplary volume trajectories, representing data and model fits, are shown in Fig. 5c and Supplementary Fig. 9. Further analysis was restricted to a reduced data set ($N = 4680$), discarding all failed optimization runs, which yield $k_{u/c} < 1$ and $\chi^2 < 50$. The resulting distribution of the fitting parameters and χ^2 is shown in Fig. 5.

Parameter distributions

Except for ϕ_{mother} the free fit parameter showed a unimodal, though partially skewed, distribution and their medians as well as their interquartile range (IQR) are listed in Table 2, together with parameter estimates from *dataset 1*. Although $t_{budstart}$ was not fitted for *dataset 2*, as it was included in the data, the parameter is listed in Table 2 for comparison.

The extensibility ϕ, which reflects the capability of the cell for plastic cell wall expansion and adjustment of the turgor pressure in the SCGM, varied drastically between *dataset 1* and *dataset 2*. While ϕ_{mother} values obtained from *dataset 2* followed a clear bimodal-distribution, values obtained from *dataset 1* showed no indication of a multimodal-distribution. Both maxima, $max(\phi_{mother}|1) = 9.6 \times 10^{-8}\,Pa^{-1}\,s^{-1}$ and $max(\phi_{mother}|2) = 7.8 \times 10^{-7}\,Pa\,s^{-1}$ were at least two magnitudes smaller than estimates from *dataset 1* and thereby closer to reported extensibility values for plant cells ($\sim 1 \times 10^{-10}\,Pa^{-1}\,s^{-1}$).[19,36] For each maximum of ϕ_{mother}, parameter sets were selected, for which ϕ_{mother} was close to this maximum, and examined for differences (Supplementary Fig. 13). Nevertheless no difference in parameter distribution could be observed. Furthermore, screening of volume trajectories for which the estimated ϕ_{mother} was either close to $max(\phi_{mother}|1)$ or $max(\phi_{mother}|2)$ (Supplementary Figs. 14 and 15) revealed no common pattern for the two groups. Whether the bimodal distribution of ϕ_{mother} results from numerical issues of the optimization algorithm or reflects two distinct population could not yet be finally clarified.

Interestingly, the ratio ϕ_{bud}/ϕ_{mother} (median (IQR)) was comparable between *dataset 2* (220(150–300)) and *dataset 1* (230 (130–8.1×10^5), underscoring that ϕ_{bud} needs to be at least 100 times higher than ϕ_{mother} to facilitate bud expansion, regardless the magnitude of ϕ. Osmolyte uptake rates k_{uptake} and ratios $k_{c/u}$ estimated from *dataset 2* were slightly higher than estimates from *dataset 1*, with $k_{uptake} = 3.0(1.9–4.2)10^{-16}\,mmol\,\mu m^{-1}\,s^{-1}$ and $k_{c/u} = 1.4(1.3–1.5)\,\mu m^{-1}$, indicating a higher single-cell growth rate and maximal volume for *dataset 2*.

The initial volume of the new born daughter, i.e. a mother with replicative age 0, is represented by its radius r_0. With $r_{0,1} = 1.2$ (1.0–1.3) µm this radius was slightly smaller for *dataset 1* than for *dataset 2*, where $r_{0,2} = 1.4(1.3–1.5)$ µm. There are several possible reasons for the discrepancy between the $r_{0,1}$, $r_{0,2}$: differences in the genome of investigated strains, experimental setup or the initial growth phase of the population. In contrast to the initial volume, the time until bud emergence $t_{budstart}$ was increased for *dataset 1* compared to *dataset 2*, with $t_{budstart,1} = 93(93–143)$ min and $t_{budstart,2} = 56(41–74)$ min. Between all fit parameters and the volume maximas of mother and bud ($maxV_{mother}$ $maxV_{bud}$), the Pearson's correlation coefficient was calculated and displayed in a correlogram (Fig. 5b). The correlation coefficients can vary by definition between −1 and 1, indicating a negative or positive correlation, whereby values close to zero represent no correlation. Except for a small correlation (0.19) for $k_{c/u}$ and k_{uptake}, the fit parameter (upper left quadrant) were uncorrelated. In contrast, the experimental volume measures and r_0 (lower right quadrant) were all positively correlated. The only correlation between volume measures and fitting parameters was found for $k_{c/u}$. Thereby $k_{c/u}$ correlated negatively to all volume measures, though the correlation was much stronger for $maxV_{mother}$ (−0.55) than for $maxV_{bud}$ (−0.27) or r_0 (−0.12). This can be explained by the cSCGM, since $k_{c/u}$ defines the maximal volume of the cell compartment, which is not reached for the bud until after cell separation.

Comparing active and passive osmotic shock responses

Adaptation to changing osmotic conditions is vital for cells. In *S. cerevisiae*, adaptation to high osmolarity is mainly achieved via increased production and retention of the small osmolyte glycerol, coordinated by the HOG pathway, through transcriptional and post-translational regulation of metabolism. We extended the SCGM by a reported description of this HOG cascade (Supplementary Note 6), comprising signaling dynamics and the activation of osmolyte production via Hog1.[27] Kinetics in the HOG cascade model were scaled according to the recently measured lower turgor pressure.[7] Additionally, we chose r_0 to be at least 1.2 µm to avoid artificially low Hog1 concentrations. Utilizing the augmented model we compared the response of the SCGM to hyperosmotic shock with and without active shock response mechanisms mediated by HOG signaling (blue and orange lines in Fig. 6).

When unperturbed (Fig. 6, dashed lines), both SCGM and SCGM with HOG establish steady states for internal osmolarity and turgor

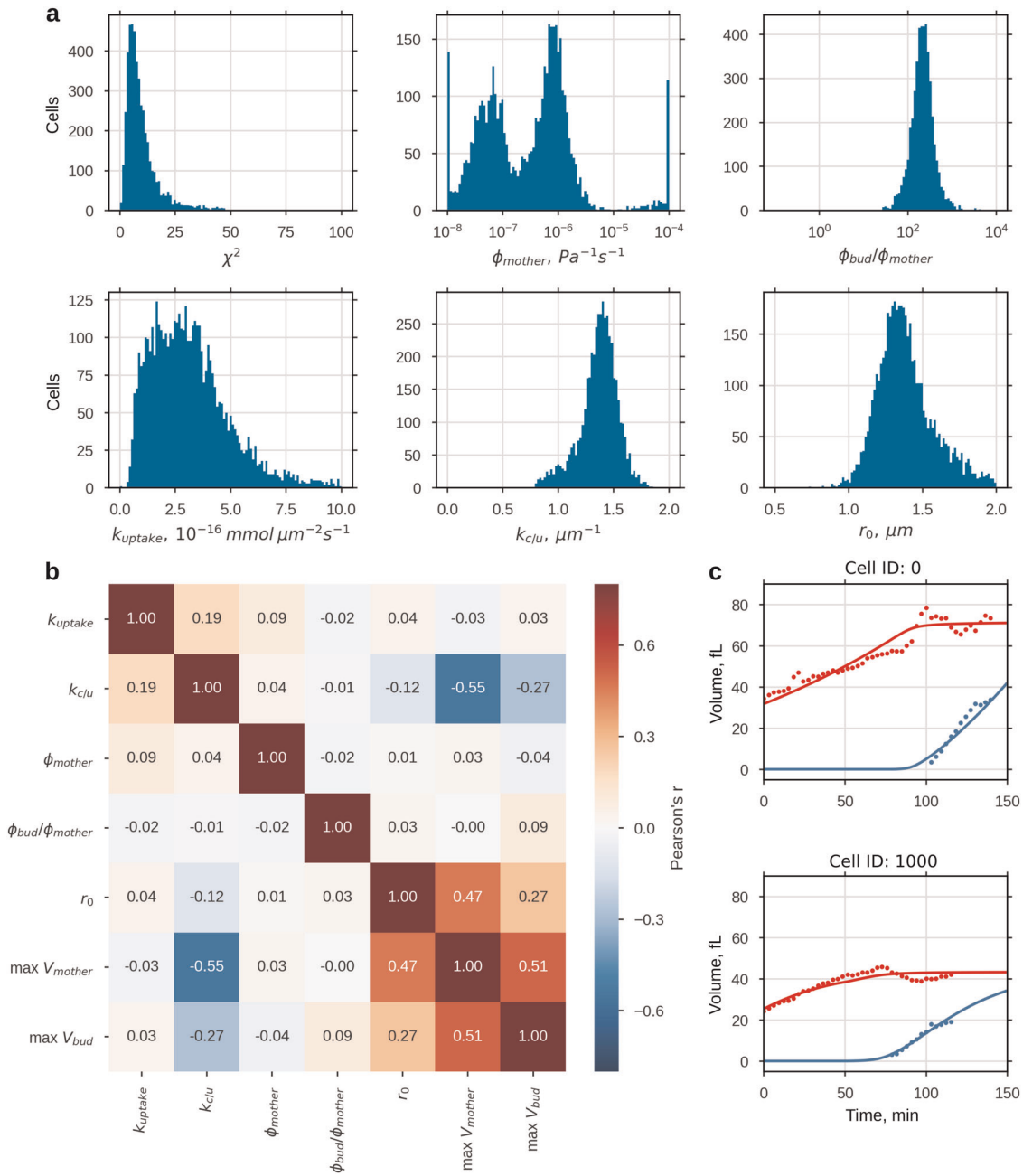

Fig. 5 cSCGM-fitted reported volume trajectories[35]. For 97% of the reported volume data for first-time mothers ($N = 6079$) a parameter set for the cSCGM could be identified. **a** Histograms of fitted parameter, excluding parameter sets where $k_u/c < 1$ µm or $\chi^2 > 50$ ($N = 4680$, histograms of complete and reduced parameter set shown in Supplementary Fig. 10). **b** Pearson's correlation of best-fitting parameters ($k_{u/c} < 1$ µm, $\chi^2 > 50$) and measured maximal volume of mother and bud, presented as correlogram, max V_{mother} and max V_{bud} were taken from the data. In **c**, two exemplary sets of measured and simulated volume trajectories are shown. Additional 24 exemplary trajectories are shown in Supplementary Fig. 9. In Supplementary Figs. 11 and 12 volume trajectories with $k_{u/c} < 1$ µm and $k_{u/c} > 1$ µm are shown

pressure while sharing comparable growth rates. However, if we simulate a hyperosmotic shock as depicted in Fig. 6a, models show an identically fast decrease in volume and turgor and a drastic increase in c_i (Supplementary Fig. 16), but the following trajectories diverge. The active response of the HOG cascade leads to production and accumulation of glycerol, which contributes to fast reestablishment of the former turgor pressure and cell size (blue line). Without the HOG cascade, cells still manage to adapt volume and turgor, but much slower. A systematic analysis of the effects of strength and timing of osmotic shock is provided in Supplementary Figs. 17 and 18.

The SCGM with HOG can reproduce previous measurements of growing yeast cells that undergo a hyperosmotic shock. In, ref. [26] cellular volume and Hog1 localization over time in response to hyperosmotic shock was measured for individual yeast cells, resulting in a phase plot that is reproduced by our model simulations (Fig. 6e). In particular, the characteristics throughout the four different phases that are reflected correctly by our approach, validate that not only the HOG response model or our volume model are functional by themselves but, more importantly, that interplay of both models is captured properly. Further, we tested whether the model also copes with hypoosmotic shock

Table 2. Estimated fit parameters of both data sets

Parameter	Unit	Factor	Median (IQR)	
			dataset 1 ($N = 21$)	*dataset 2* ($N = 4680$)
k_{uptake}	$\frac{mmol}{\mu m^2\,s}$	10^{-16}	1.4 (1.0–1.9)	3.0 (1.9–4.2)
$k_{c/u}$	$\frac{1}{\mu m}$		1.21 (1.18–1.27)	1.4 (1.3–1.5)
ϕ_{mother}	$\frac{1}{Pa\,s}$	10^{-4}	5.5 (3.1–6.8)	–
ϕ_{bud}/ϕ_{mother}		10^{2}	2.3 (1.3–8.1 × 10^3)	2.2 (1.5–3.0)
r_0	µm		1.2 (1.0–1.3)	1.4 (1.3–1.5)
$t_{budstart}$	min	10^{1}	9.3 (9.3–14.3)	5.6 (4.1–7.4)

$t_{budstart}$ of *dataset 2* was provided by the data. ϕ_{mother} showed bimodal distribution and was neglected in this table

(Fig. 6a, c). Again model integrity is restored following a first hyperosmotic shock and, thus, regains osmolarity and volume after a second, now hypoosmotic, shock. Obviously, hypoosmotic shock results in a short overshoot of cell size (Fig. 6c), as previously reported in ref. [37] Hyperosmotic shock exclusively leads to elastic deformation, while hypoosmotic shock leads to negligibly small plastic deformation. Both types of osmotic shock induce elastic behavior of the cell wall, hence the modeled cell would not grow effectively through step-like osmotic changes of the environment.

The reference volume (Fig. 6f and Supplementary Note 1 for definition) quantifies growth as it integrates plastic deformation of the cell wall under normal conditions reflecting a elasto-viscoplastic behavior (EP) (Fig. 6f, white area). In contrast, a hyperosmotic shock induces immediate cell shrinkage and stops growth, as indicated by the reference volume. The reference volume remains constant, since the elasto-viscoplastic regime is left and the model behaves ideal-elastically (E) (Fig. 6f, gray area).

DISCUSSION

Knowledge of single-cell growth dynamics is crucial for the understanding of comprehensive biological systems, particularly for model systems such as *S. cerevisiae*. Here, we introduced and justified a volume model of yeast by integrating different theoretical concepts of cell mechanics, integrity, and osmolyte dynamics in combination with experimental data on single cell growth and cell wall elasticity. The model applies to several scenarios, where cell size variation plays a role: from growth of an individual bud connected to the mother cell, the case of a two-bud growing mutant of yeast, and the direct and long-term volume response after hyperosmotic shock.

In previous studies, two modes of single-cell growth were considered for yeast, linear and exponential.[38–41] Based on our model we proposed a more complex picture of the specific growth pattern of a single yeast cell (Fig. 1b). We derived an exact analytic solution for the cellular radius over time $r(t)$ for a single undisturbed-growing cell. Prospectively, this solution may support future work as it relates relevant parameters, which originate from formerly distinct concepts, such as cell wall mechanics, water homeostasis, and osmoregulation, in the form of a single expression describing the growth of an individual cell overall. This expression allows us to deduce properties of the described system in a closed form. Specifically, we exemplified such a deduction by calculating the limes of the radius for long time spans $r_{t\to\infty}$. The approach revealed that the maximal cell size is determined by the ratio $k_{u/c}$ of osmolyte or nutrient uptake and consumption, but is independent of mechanical cell wall properties, such as Young's modulus or extensibility. We assumed yeast cells to be spherical, though their true shape might be better described as rotational ellipsoid. Introducing such ellipsoidal geometry would drastically complicate the model, as the assumption of a uniform stress inside the cell wall does not hold anymore and local stresses have to be considered. We argue even for rotational-ellipsoidal cells with rather small differences between major and minor axes, the approximation of a sphere is sufficient to capture the geometric impact on cell growth. Besides the cell wall mechanic, an ellipsoidal geometry would impact the osmolyte uptake, as it scales with the cell surface. Although the surface of a rotational ellipsoid is always bigger than that of a sphere, both surface-volume ratios follow the same trend (Supplementary Fig. 4). Therefore, the fitted values for k_{uptake} might be overestimated, but the growth dynamic is preserved.

The SCGM works fully without a connection to the cell cycle machinery comprising the action of cyclins, CDKs, and CK1. Nevertheless, the coupled SCGM is not independent of cell cycle, since the characteristic length of first cell cycle is integrated via $t_{budstart}$. Parameterizing the SCGM with measured volume trajectories we found that this characteristic cell cycle length varied significantly between individual cells.

Yeast cells proliferate by budding, a process in which a larger mother and a smaller bud grow simultaneously but with different growth rates. To describe this coordinated growth, two instances of the SCGM with different initial volumes were coupled by allowing water and osmolyte fluxes between the instances. For simplicity, we neglected the specific bud localization at the mother, which would include the complex polarization process.[42,43] This coupled SCGM can be interpreted as an augmented model compared to a previous description of interconnected soap bubbles or balloons.[29,44] However, those models lack the exchange of matter with their environment which is crucial for biological applications. In the coupled SCGM we allowed fluxes in-between the compartments and between compartments and medium such that our model operates near equilibrium instead of being at equilibrium. Plastic and elastic cell wall expansion depend on the lateral stresses, which scales with radius and acting pressure. To allow expansion of the smaller of the two volumes, the cell wall of that volume must be either more elastic (E) or more extendable (ϕ).

Utilizing AFM, we could reject the hypothesis that elasticity is the distinguishing cell wall property between mother and bud. The measured local Young's modulus at the bud was not lower but similar or even slightly higher compared to the mother. Therefore, we inferred, from the SCGM, that ϕ must be significantly higher at the bud to facilitate bud expansion. Fitting the coupled SCGM to the growth data suggests that ϕ_{mother} is three orders of magnitude higher than reported values for plants[45,46] and ϕ_{bud} needs to be at least two magnitudes higher than at mother cell wall. Furthermore, we have shown that significantly increased ϕ_{bud} compared to ϕ_{mother} can explain the observed higher growth rates of buds.[30] The higher extensibility of the bud cell wall might be caused by incorporation of new more expandable material, which maturates over time or by subsequent alterations of the already formed cell wall. Plant enzymes are reported to alter mechanical cell wall properties,[47,48] thereby influencing growth and cell shape.[49] Further reports also suggest that cell wall plasticity in fungi is controlled by hydrolytic enzymes, like chitinases or glucanases.[5,50–52] The higher extensibility of the bud cell wall could also reflect the orientation of the cytoskeleton towards the emerging bud,[53] which directs new cell wall material predominantly to that bud. Fitting the coupled model to single-cell volume trajectories from two completely independent data sets enabled us to estimate crucial growth parameters, such as the global osmolyte uptake rate k_{uptake} and the ratio $k_{u/c}$. Both parameters appeared to be very sensitive, as k_{uptake} had the strongest impact on individual growth rate and $k_{u/c}$ on the maximum cell volume. From comparison of both data sets, two main observations can be stated: First, cell expansion of *S. cerevisiae*, under non-limiting conditions, requires a total osmolyte uptake rate of 1.0–4.0 mmol $\mu m^{-2}\,s^{-1}$ and a

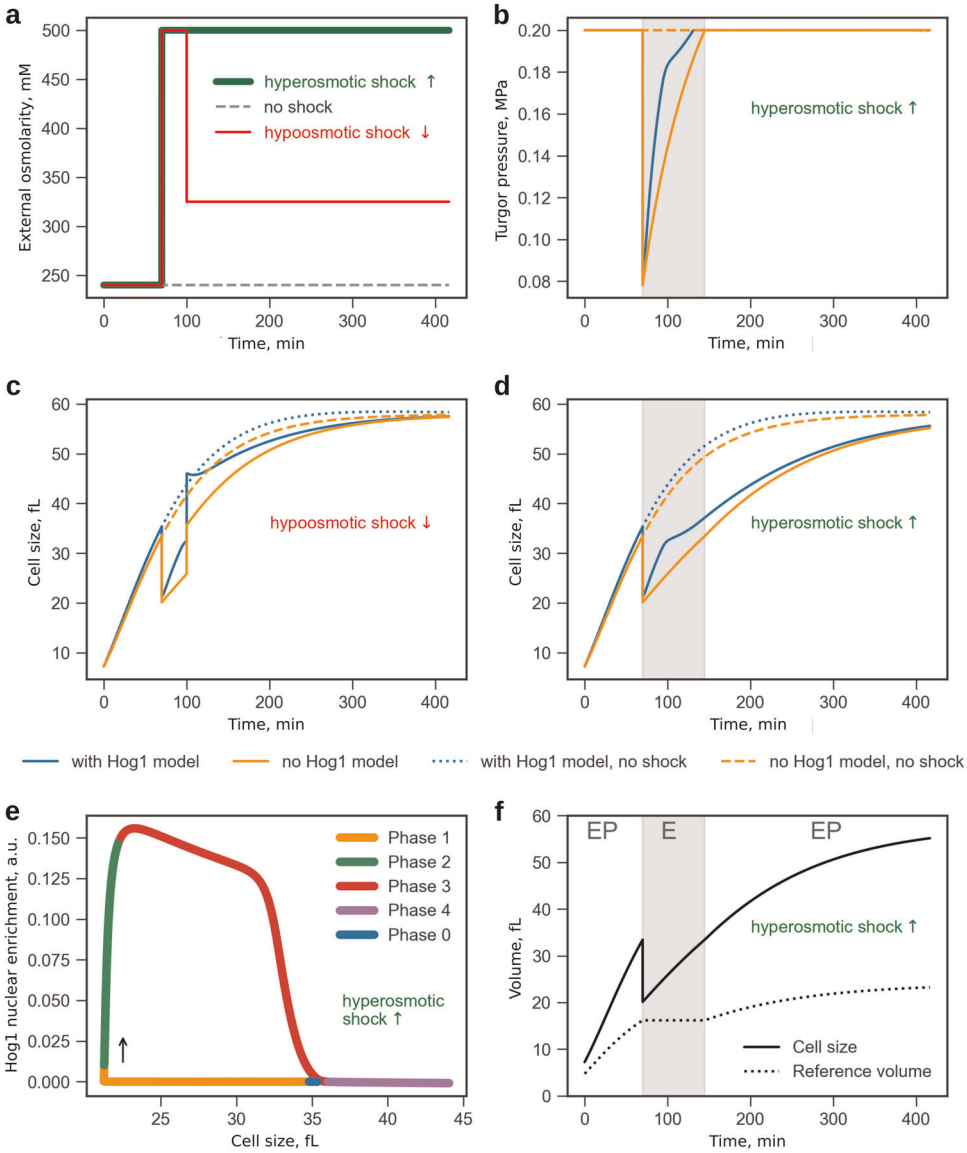

Fig. 6 Growing single cell exposed to osmotic shocks. Simulation of our SCGM with a HOG response model reproduces Hog1-signaling behavior in growing yeast cells. We compared SCGM dynamics upon hyper-osmotic and hypo-osmotic shock with and without active response mechanism. **a** Shock scenarios: no shock (black dashed line), single hyperosmotic shock (external osmolarity raised to 500 mM at 70 min, green line), and combination of hyper-osmotic and hypo-osmotic shock (external osmolarity is raised to 500 mM at 70 min and reduced to 325 mM at 100 min, red line). (**b**–**d**) Shock response (**b**, **d**—only hyperosmotic, **c** hyper-osmotic and hypo-osmotic) with (blue lines) and without (orange lines) active HOG response. **b** Shows turgor pressure, which drops and re-adapts with and without signaling, but faster with signaling. **c**, **d** Show cell size, which also adapts faster to stress in case of active HOG response. **e** Short-term and long-term response of the model with HOG response to the same hyperosmotic shock as in **b**, **d** showing Hog1 nuclear enrichment versus cell size trajectory as four distinct phases of response behavior after shock (indicated as phase zero) as proposed by Muzzey et al. [26]: (1) passive but fast shrinkage and turgor loss, (2) activation of Hog1 signaling, (3) restoration of cell size and turgor pressure, and finally (4) resuming cellular growth. Our model reflects these phases and combines the fast timescale in (1) (volume loss within a few seconds) and steady growth either without a shock or due to adaption after shock as in the last phase. **f** Comparison of cell size to reference volume (shock as in **b**, **d**). The reference volume reflects the distinct cell wall mechanic regimes of our model: elasto-plastic behavior (EP) during growth, ideal elastic behavior (E, gray area) in response to hyperosmotic shock, and growth resumption (EP) after restoring former size and turgor pressure (see turgor trajectory in **b**)

consumption rate which is 1.2–1.5 μm^{-1} times higher. Second, the extensibility of the bud cell wall has to be at least 100 higher than the mother's, to facilitate bud expansion.

Intriguingly, the estimated osmolyte uptake rates k_{uptake} were only two to five times higher than the average glucose uptake rate per surface area under aerobic conditions reported by Jouhten et al. [54] (see Supplementary Note 5). Under these conditions glucose would account for 30–60% of the osmolytes taken up by the cell, revealing a new angle on the impact of glucose onto cellular growth: So far the impact of glucose onto cell growth based exclusively on the fact that glucose is a main nutrient source, providing chemical energy and building blocks for macromolecules, and hence can be regarded as fuel of the cell. While this study indicates, that additionally to those aspects, the massive glucose import could drive water influx and hence contribute significantly to cell expansion.

In general, the cSCGM described very well the volume expansion of different single-cell trajectories, which have been measured in microfluidic growth experiments. Using the cSCGM, we could also recapitulate earlier experimental data presented by

Soifer et al. [39] and resulting relations between division time and ratio of volumes at division and birth (Supplementary Fig. 5), despite different interpretation for the growth dynamics of single cells.

By integrating the osmotic stress response, specifically the HOG-signaling pathway and metabolic adaptation from ref. [27], in the SCGM, we could compare the passive volume adaptation with the active response arising from the HOG pathway. This model was able to capture the different time scales ranging from steady growth to the drastic shrinkage of cell size followed by an osmotic shock. To our knowledge, this is the first time that the joint-dynamics of Hog1 enrichment versus volume following a hyperosmotic shock[26] could be reproduced and explained by a mathematical model. Additionally, our model can describe the response to hypoosmotic shock similarly to previous reports.[37] The simulations illustrate the functionality of the coupled model over a wide range of cell sizes. However, validity of the combined model is limited in cases of tiny initial volume (e.g. 1 fL), since the Zi-model assumes fixed numbers of Hog1 molecules. During growth, increasing volume results in dilution of all species within the HOG model and, hence, would lead to non-physiologically small concentrations for tiny initial volumes. To overcome such limiting effects, production rates for all species of the HOG model need to be introduced and parameterized to counteract the dilution process. Instead, we chose a simplistic implementation of coupling both models, in order to preserve their original properties.

In this study, we focused on single-cell growth of newly budded yeast cells and their volume dynamics. Extending the cSCGM to cover several cell cycles with several consecutive budding events and test it against experimental data might help to understand the interplay of morphogenesis and aging of *S. cerevisiae*. A next step would be the combination of the SCGM with models focusing on cell cycle regulation or polarization into larger models to investigate the interplay between regulatory networks and growth. Mathematical models for growth dynamics at the population level are often based on greatly simplified single cell volume models.[55,56] The presented SCGM might help to improve such models and increase our understanding of population growth dynamics.

METHODS

Yeast strains

For the microfluidic growth analysis we used a *S. cerevisiae* strain based on BY4742 (MAT*α*his3Δ1 leu2Δ0 lys2Δ0 ura3Δ0),[57] in which the bud neck marker Cdc10 has been genomically labeled with mKate2. The sequence of mKate2 was cloned into the plasmid pUG72 (Euroscarf) and Cdc10 was labeled using PCR-based homologous recombination. The necessary Ura3 marker cassette has been removed using the Cre-loxP recombination system.[58] In the nano-indentation experiments we used the strain BY4741.[57]

Yeast cell culture

For the microfluidic growth experiments, cells were grown at 30 °C overnight in synthetic medium (SD; 0.17% yeast nitrogen base without amino acids, 0.5% ammonium sulfate, 2% glucose, 55 mg/L adenine, 55 mg/L L-tyrosine, 55 mg/L uracil, 20 mg/L L-arginine, 10 mg/L L-histidine, 60 mg/L L-isoleucine, 60 mg/L L-leucine, 40 mg/L L-lysine, 10 mg/L L-methionine, 60 mg/L phenylalanine, 50 mg/L L-threonine, and 40 mg/L L-tryptophan). Medium osmolarity was measured with an osmometer (gonotec, Berlin, Germany). Before the experiment, 500 µL of overnight culture were diluted in 5 mL SD medium and grown for 2.5 h at 30 °C.

Microfluidic growth experiments

We used the CellASIC ONIX microfluidic platform (Merck Millipore, Darmstadt, Germany) with the haploid yeast plates (Y04C) for growth analysis. Plates were primed with SD medium and cells were loaded as described in the ONIX yeast protocol. Flow control pressure was set to 2 psi. Cells were observed using a Visitron Visiscope inverted spinning disc laser confocal microscope (Visitron, Puchheim, Germany). The temperature of the microfluidic plate was controlled to 30 °C using a temperature control chamber (OL IX73/83 cellVivo, PeCon GmbH, Erbach, Germany). We used a 150× oil immersion objective (Olympus UPlanSApo 150X/1.47, Oil, TIRM) and the Photometrics Evolve 512 EMCCD camera (Photometrics, Tuscon, USA). Fluorescent illumination was provided by a 561 nm diode laser and a multibad dichroic filter (405/488/559/635 nm) together with a 600/50 nm emission filter for detection. A brightfield image was taken every 3 min, while a fluorescent image was only taken every 12 min, to minimize fluorescent exposure of cells. Each image was acquired as a z-stack (six z-positions, 0.5 µm distance).

Image analysis

For each z-stack, the sharpest plane was determined using the ImageJ plugin "Find focused slices" by Quingzong Tseng. Brigthfield images were segmented and cells were tracked with the CellProfiler[59] plugin Cellstar.[34] Tracking was manually checked, and mis-tracked cells were removed from the analysis. For each cell, bud appearance time was manually defined as the time when a bud was first visible in the brightfield image. The lineage was manually determined using the fluorescent images of the bud neck marker Cdc10-mKate2. Cell area was converted to volume by assuming a spherical cell shape.

Cell wall nano-indentation

In brief, log-phase yeast cells were mechanically trapped in porous polycarbonate membrane, with pore size of 5 µm.[60] The cell-containing membrane was subsequently immobilized on the bottom of a liquid chamber and probed with an AFM (Nanowizard III, JPK, Germany). All AFM measurements were conducted in liquid solution of synthetic media using MLCT-E cantilever (Bruker). Prior to all experiments, the spring constant was determined via thermal noise method. Multiparametric imaging of cells was done using the provided QI-Mode, whereby maximal applied force was set to 1 nN, corresponding to an indentation depth of ~35 nm. For further analysis we used JPK data-processing software and the Python packages numpy, scipy[61] or pandas.[62] For a more detailed description see ref. [7]

DATA AVAILIBILITY

The SCGM and the coupled SCGM are available as antimony model under: https://github.com/tbphu/volume_model/blob/SCGM/volume_mother_and_bud.txt and https://github.com/tbphu/volume_model/blob/master/volume_reference_radius.txt. The first dataset, measured and analyzed during the current study, is available under https://github.com/tbphu/cellsize, while the second analyzed dataset was published by[35] and is available under http://charvin.igbmc.science/yeastcycledynamics/.

Received: 28 March 2019; Accepted: 23 August 2019;
Published online: 26 September 2019

REFERENCES

1. Kedem, O. & Katchalsky, A. Thermodynamic analysis of the permeability of biological membranes to non-electrolytes. *Biochim. Biophys. Acta* **27**, 229–246 (1958).
2. Hohmann, S. Osmotic adaptation in yeast—control of the yeast osmolyte system. *Int. Rev. Cytol.* **215**, 149–187 (2002).
3. Klipp, E., Nordlander, B., Krüger, R., Gennemark, P. & Hohmann, S. Integrative model of the response of yeast to osmotic shock. *Nat. Biotechnol.* **23**, 975–982 (2005).
4. Schaber, J. et al. Biophysical properties of *Saccharomyces cerevisiae* and their relationship with HOG pathway activation. *Eur. Biophys. J.* **39**, 1547–1556 (2010).
5. Klis, F. & Mol, P. Dynamics of cell wall structure in *Saccharomyces cerevisiae*. *FEMS Microbiol. Rev.* **26**, 239–256 (2002).
6. Proctor, S. A., Minc, N., Boudaoud, A. & Chang, F. Contributions of turgor pressure, the contractile ring, and septum assembly to forces in cytokinesis in fission yeast. *Curr. Biol.* **22**, 1601–1608 (2012).
7. Goldenbogen, B. et al. Dynamics of cell wall elasticity pattern shapes the cell during yeast mating morphogenesis. *Open Biol.* **6**, 160136 (2016).
8. Jiang, H. & Sun, S. X. Cellular pressure and volume regulation and implications for cell mechanics. *Biophys. J.* **105**, 609–619 (2013).

9. Tao, J. & Sun, S. X. Active biochemical regulation of cell volume and a simple model of cell tension response. *Biophys. J.* **109**, 1541–1550 (2015).
10. Smith, A. E., Moxham, K. & Middelberg, A. P. J. On uniquely determining cell–wall material properties with the compression experiment. *Chem. Eng. Sci.* **53**, 3913–3922 (1998).
11. Smith, A. E., Moxham, K. E. & Middelberg, A. P. J. Wall material properties of yeast cells. Part II. Analysis. *Chem. Eng. Sci.* **55**, 2043–2053 (2000a).
12. Smith, A. E., Zhang, Z. & Thomas, C. R. Wall material properties of yeast cells: Part 1. Cell measurements and compression experiments. *Chem. Eng. Sci.* **55**, 2031–2041 (2000).
13. Smith, A. E., Zhang, Z., Thomas, C. R., Moxham, K. E. & Middelberg, A. P. The mechanical properties of *Saccharomyces cerevisiae*. *Proc. Natl Acad. Sci. USA* **97**, 9871–9874 (2000).
14. Stenson, J. D., Thomas, C. R. & Hartley, P. Modelling the mechanical properties of yeast cells. *Chem. Eng. Sci.* **64**, 1892–1903 (2009).
15. Stenson, J. D., Hartley, P., Wang, C. & Thomas, C. R. Determining the mechanical properties of yeast cell walls. *Biotechnol. Prog.* **27**, 505–512 (2011).
16. Cosgrove, D. Analysis of the dynamic and steady-state responses of growth rate and turgor pressure to changes in cell parameters. *Plant Physiol.* **68**, 1439–1446 (1981).
17. Dumais, J., Shaw, S. L., Steele, C. R., Long, S. R. & Ray, P. M. An anisotropic-viscoplastic model of plant cell morphogenesis by tip growth. *Int. J. Dev. Biol.* **50**, 209–222 (2006).
18. Ortega, J. & Welch, S. Mathematical models for expansive growth of cells with walls. *Math. Model. Nat. Phenom.* **8**, 35–61 (2013).
19. Ortega, J. K. Augmented growth equation for cell wall expansion. *Plant Physiol.* **79**, 318–320 (1985).
20. Ortega, J. K., Zehr, E. G. & Keanini, R. G. In vivo creep and stress relaxation experiments to determine the wall extensibility and yield threshold for the sporangiophores of phycomyces. *Biophys. J.* **56**, 465–475 (1989).
21. Ortega, J. K. E. et al. A comparison of cell-wall-yielding properties for two developmental stages of *Phycomyces sporangiophores* determination by in-vivo creep experiments. *Planta* **183**, 613–619 (1991).
22. Boudaoud, A. Growth of walled cells: from shells to vesicles. *Phys. Rev. Lett.* **91**, 018104 (2003).
23. Chang, F. & Huang, K. How and why cells grow as rods. *BMC Biol.* **12**, 54 (2014).
24. Case, J., Chilver, H. C. & Ross, C. T. F. Thin shells under internal pressure. In *Strength of Materials and Structures*, 152–168 (Butterworth-Heinemann, 1999).
25. Strange, K. Cellular volume homeostasis. *Adv. Physiol. Educ.* **28**, 155–159 (2004).
26. Muzzey, D., Gómez-Uribe, C. A., Mettetal, J. T. & van Oudenaarden, A. A systems-level analysis of perfect adaptation in yeast osmoregulation. *Cell* **138**, 160–171 (2009).
27. Zi, Z., Liebermeister, W. & Klipp, E. A quantitative study of the Hog1 MAPK response to fluctuating osmotic stress in *Saccharomyces cerevisiae*. *PLoS ONE* **5**, e9522 (2010).
28. Geitmann, A. & Ortega, J. K. E. Mechanics and modeling of plant cell growth. *Trends Plant Sci.* **14**, 467–478 (2009).
29. Merritt, D. R. & Weinhaus, F. The pressure curve for a rubber balloon. *Am. J. Phys.* **46**, 976–977 (1978).
30. Ferrezuelo, F. et al. The critical size is set at a single-cell level by growth rate to attain homeostasis and adaptation. *Nat. Commun.* **3**, 1012 (2012).
31. Cabib, E., Roh, D. H., Schmidt, M., Crotti, L. B. & Varma, A. The yeast cell wall and septum as paradigms of cell growth and morphogenesis. *J. Biol. Chem.* **276**, 19679–19682 (2001).
32. Francois, J. M. et al. Use of atomic force microscopy (AFM) to explore cell wall properties and response to stress in the yeast *Saccharomyces cerevisiae*. *Curr. Genet.* **59**, 187–196 (2013).
33. Touhami, A., Hoffmann, B., Vasella, A., Denis, F. A. & Dufrêne, Y. F. Aggregation of yeast cells: direct measurement of discrete lectin–carbohydrate interactions. *Microbiology* **149**, 2873–2878 (2003).
34. Versari, C. et al. Long-term tracking of budding yeast cells in brightfield microscopy: CellStar and the evaluation platform. *J. R. Soc. Interface* **14**, https://doi.org/10.1098/rsif.2016.0705 (2017).
35. Garmendia-Torres, C., Tassy, O., Matifas, A., Molina, N. & Charvin, G. Multiple inputs ensure yeast cell size homeostasis during cell cycle progression. *eLife* **7**, e34025 (2018).
36. Cosgrove, D. J. Cell wall yield properties of growing tissue. *Plant Physiol.* **78**, 347–356 (1985).
37. Talemi, S. R. et al. Systems level analysis of the yeast osmo-stat. *Sci. Rep.* **6**, 30950 (2016).
38. Mitchison, J. The growth of single cells. *Exp. Cell Res.* **15**, 214–221 (1958).
39. Soifer, I., Robert, L. & Amir, A. Single-cell analysis of growth in budding yeast and bacteria reveals a common size regulation strategy. *Curr. Biol.* **26**, 356–361 (2016).
40. Turner, J. J., Ewald, J. C. & Skotheim, J. M. Cell size control in yeast. *Curr. Biol.* **22**, R350–R359 (2012).
41. Tyson, J. J. & Hannsgen, K. B. Global asymptotic stability of the size distribution in probabilistic models of the cell cycle. *J. Math. Biol.* **22**, 61–68 (1985).
42. Chiou, J.-G., Balasubramanian, M. K. & Lew, D. J. Cell polarity in yeast. *Annu. Rev. Cell Dev. Biol.* **33**, 77–101 (2017).
43. Giese, W., Eigel, M., Westerheide, S., Engwer, C. & Klipp, E. Influence of cell shape, inhomogeneities and diffusion barriers in cell polarization models. *Phys. Biol.* **12**, 066014 (2015).
44. Weinhaus, F. & Barker, W. On the equilibrium states of interconnected bubbles or balloons. *Am. J. Phys.* **46**, 978–982 (1978).
45. Ortega, J. Dimensionless number is central to stress relaxation and expansive growth of the cell wall. *Sci. Rep.* **7**, 1–16 (2017).
46. Taiz, L. Plant cell expansion: regulation of cell wall mechanical properties. *Annu. Rev. Plant Physiol.* **35**, 585–657 (1984).
47. Cosgrove, D. Loosening of plant cell walls by expansins. *Nature* **407**, 321–326 (2000).
48. Cosgrove, D. J. Enzymes and other agents that enhance cell wall extensibility. *Annu. Rev. Plant Physiol. Plant Mol. Biol.* **50**, 391–417 (1999).
49. Okamoto-Nakazato, A. Distribution of yieldin, a regulatory protein of the cell wall yield threshold, in etiolated cowpea seedlings. *Plant Cell Physiol.* **42**, 952–958 (2001).
50. Adams, D. J. Fungal cell wall chitinases and glucanases. *Microbiology* **150**, 2029–2035 (2004).
51. Duo-Chuan, L. Review of fungal chitinases. *Mycopathologia* **161**, 345–360 (2006).
52. Klis, F. M., Boorsma, A. & De Groot, P. W. J. Cell wall construction in *Saccharomyces cerevisiae*. *Yeast* **23**, 185–202 (2006).
53. Slaughter, B. D., Smith, S. E. & Li, R. Symmetry breaking in the life cycle of the budding yeast. *Cold Spring Harb. Perspect. Biol.* **1**, a003384 (2009).
54. Jouhten, P. et al. Oxygen dependence of metabolic fluxes and energy generation of *Saccharomyces cerevisiae* CEN.PK113-1A. *BMC Syst. Biol.* https://doi.org/10.1186/1752-0509-2-60. (2008).
55. Spiesser, T. W., Müller, C., Schreiber, G., Krantz, M. & Klipp, E. Size homeostasis can be intrinsic to growing cell populations and explained without size sensing or signalling. *FEBS J.* **279**, 4213–4230 (2012).
56. Spiesser, T. W., Kühn, C., Krantz, M. & Klipp, E. Bud-localization of CLB2 mRNA can constitute a growth rate dependent daughter sizer. *PLoS Comput. Biol.* https://doi.org/10.1371/journal.pcbi.1004223 (2015).
57. Brachmann, C. B. et al. Designer deletion strains derived from *Saccharomyces cerevisiae* S288C: a useful set of strains and plasmids for PCR-mediated gene disruption and other applications. *Yeast* **14**, 115–132 (1998).
58. Hegemann, J. H. & Heick, S. B. Delete and repeat: a comprehensive toolkit for sequential gene knockout in the budding yeast *Saccharomyces cerevisiae*. *Methods Mol. Biol.* **765**, 189–206 (2011).
59. Carpenter, A. E. et al. CellProfiler: image analysis software for identifying and quantifying cell phenotypes. *Genome Biol.* **7**, R100 (2006).
60. Kasas, S. & Ikai, A. A method for anchoring round shaped cells for atomic force microscope imaging. *Biophys. J.* **68**, 1678–1680 (1995).
61. van der Walt, S., Colbert, S. C. & Varoquaux, G. The NumPy Array: a structure for efficient numerical computation. *Comput. Sci. Eng.* **13**, 22–30 (2011).
62. Mckinney, W. Data structures for statistical computing in Python. In *Proc. 9th Python in Science Conference* (eds van der Walt, S. & Millman, J.) 51–56 (2010).
63. Dupres, V., Dufrêne, Y. & Heinisch, J. Measuring cell wall thickness in living yeast cells using single molecular rulers. *ACS Nano* **4**, 5498–5504 (2010).

ACKNOWLEDGEMENTS

This work was supported by the Deutsche Forschungsgemeinschaft (DFG) through Collaborative Research Center (SFB740 to E.K.), the excellence cluster (MATH$^+$ to B.G. and E.K.) and by project "Osmotic stress regulation" (UH 279/1-1 to J.U.).

AUTHOR CONTRIBUTIONS

T.A., B.G. and E.K. conceived the project. T.A. formulated the models, which were refinied by B.G. and J.U. B.G. and J.U. conducted all experiments and analyzed the data. T.A., B.G. and E.K. wrote the paper.

COMPETING INTERESTS

The authors declare no competing interests.

ADDITIONAL INFORMATION

Supplementary information is available for this paper on the *npj Systems Biology and Applications* website (https://doi.org/10.1038/s41540-019-0111-6).

Correspondence and requests for materials should be addressed to E.K.